Mapping Reduced Accessibility to WASH Facilities in Rohingya Refugee Camps with Sub-Meter Imagery

Kyeongjin Ahn^{1,2,†} YongHun Suh^{1,†} Sungwon Han³ Jeasurk Yang^{1,*} Hannes Taubenböck^{4,5,*} Meeyoung Cha^{1,2,*}

¹Data Science for Humanity Group, Max Planck Institute for Security and Privacy (MPI-SP), Bochum, Germany

²School of Computing, Korea Advanced Institute of Science and Technology (KAIST), Daejeon, Republic of Korea

> ³Meta, California, United States

⁴German Aerospace Center (DLR), Earth Observation Center (EOC), Weßling, Germany

⁵Institute of Geography and Geology, Earth Observation Research Cluster (EORC), Würzburg University, Würzburg, Germany

[†]These authors contributed equally as first authors: kyeongjin.ahn@kaist.ac.kr; yong-hun.suh@mpi-sp.org.
*Corresponding authors: jeasurk.yang@mpi-sp.org; hannes.taubenboeck@dlr.de; mia.cha@mpi-sp.org.

ABSTRACT

Access to Water, Sanitation, and Hygiene (WASH) services remains a major public health concern in refugee camps. This study introduces a remote sensing-driven framework to quantify WASH accessibility—specifically to water pumps, latrines, and bathing cubicles—in the Rohingya camps of Cox's Bazar, one of the world's most densely populated displacement settings. Detecting refugee shelters in such emergent camps presents substantial challenges, primarily due to their dense spatial configuration and irregular geometric patterns. Using sub-meter satellite images, we develop a semi-supervised segmentation framework that achieves an F1-score of 76.4% in detecting individual refugee shelters. Applying the framework across multi-year data reveals declining WASH accessibility, driven by rapid refugee population growth and reduced facility availability, rising from 25 people per facility in 2022 to 29.4 in 2025. Gender-disaggregated analysis further shows that women and girls experience reduced accessibility, in scenarios with inadequate safety-related segregation in WASH facilities. These findings suggest the importance of demand-responsive allocation strategies that can identify areas with under-served populations—such as women and girls—and ensure that limited infrastructure serves the greatest number of people in settings with fixed or shrinking budgets. We also discuss the value of high-resolution remote sensing and machine learning to detect inequality and inform equitable resource planning in complex humanitarian environments.

Keywords refugee · segmentation · remote sensing · accessibility · Rohingya

1 Introduction

Forced displacement of populations due to armed conflicts, environmental hazards, and systemic persecution pose pressing humanitarian and public health challenges worldwide [1]. As of 2024, the United Nations High Commissioner for Refugees (UNHCR) estimated that the global population of forcibly displaced individuals, including both Internally Displaced People (IDP) and refugees, had reached approximately 123 million [2]. Among these, the displacement of the Rohingya population from Myanmar represents one of the most protracted and densely concentrated refugee situations in recent history [3]. Following the escalation of violence in Myanmar's Rakhine State in 2017, over one million Rohingya individuals have fled to Bangladesh, leading to a rapid formation of refugee settlements in the Cox's Bazar District [4]. The Government of Bangladesh designates these individuals as Forcibly Displaced Myanmar Nationals (FDMNs), who are currently accommodated in 33 camps occupying a total area of 24 square kilometers. By May 2025, these camps are known to host over 1.1 million individuals, with an average density exceeding 45,000 persons per square kilometer [5]. This would make the camp the third largest city in Germany by population, while its area would correspond to that of a town with around 5,000 inhabitants.

This extreme concentration of displaced persons put considerable strain on infrastructure and service delivery, particularly in the domains of water, sanitation, and hygiene (WASH), lack of which can lead to elevated risks of communicable diseases, including waterborne infections and dermatological conditions [6, 7]. These risks are disproportionately borne by vulnerable subpopulations, notably women and children, exposing the urgent need for sustained humanitarian intervention [8]. However, detailed assessments of such basic living conditions remain limited. Prior studies have documented access to essential services through surveys of selected camps [9, 10], leaving the broader spatial distribution and magnitude of deficiencies unknown.

To inform evidence-based resource allocation and generate data estimates for humanitarian stakeholders, this study presents a spatial analysis of access to basic services across the Rohingya refugee camps. While multiple dimensions of camp infrastructure—such as shelter quality, education, and healthcare access—warrant systematic monitoring, we focus on WASH facilities due to their critical role in mitigating public health risks and upholding the dignity and well-being of displaced populations [11]. To support this analysis, we utilized two comprehensive datasets from 2022 and 2024 [12], which document three categories of WASH infrastructure (i.e., water pumps, latrines, and bathing cubicles) corresponding to water, sanitation, and hygiene services, respectively. By estimating year-by-year changes of WASH supply, this analysis identifies spatial and temporal disparities in service provision and pinpoints areas with the highest unmet needs, demonstrating the potential to guide targeted humanitarian interventions.

We employ remote sensing technologies to derive structural information. Refugee shelters often exhibit structural characteristics that differ significantly from those of typical urban environments [13]. Computer vision segmentation algorithms have offered high performance capabilities for accurately delineating refugee shelter outlines from high-resolution satellite imagery [14]. However, detecting shelters within Rohingya refugee camps presents a much greater challenge than in other humanitarian contexts. In a global comparative study of camp structures [15], many United Nations—managed camps were found to have standardized layouts, where shelters are regularly spaced, making them relatively easy to identify via remote sensing [16]. By contrast, the Rohingya camps are densely clustered, irregularly aligned, and situated on hilly terrain, with shelters constructed in extremely close proximity. Therefore, more robust models are required to detect the shelters with high compactness and low geometric alignment.

This study adopts a two-stage methodological framework to map uneven accessibility to WASH facilities in the Rohingya refugee camps. First, we develop a semi-supervised segmentation framework for refugee shelter detection using sub-meter resolution satellite imagery. Manually digitized shelter outline data by the United Nations Satellite Centre (UNOSAT) and REACH initiative [17] are used to train the framework, enabling the detection of shelters from various remote sensing sources such as Unmanned Aerial Vehicles (UAV) and Very High Resolution (VHR) satellite images collected between 2017 and 2025. In the second stage, we calculate accessibility scores for the detected shelters relative to the three types of WASH facilities in 2022 and 2024. In particular, the 2022 data for latrines and bathing cubicles are further categorized by gender (male, female, and all-gender), allowing comparative analysis of accessibility by gender. To calculate accessibility, we employ an enhanced version of the Two-Step Floating Catchment Area (2SFCA) method [18, 19]. 2SFCA considers both the supply of facilities and the spatial distribution of the population, providing a more realistic measure of accessibility than traditional proximity-based methods [20, 21].

Beyond the immediate case study, our framework has direct operational value for the coordination and policy of refugee response. In humanitarian programming, budgets and facility stocks are typically fixed or slow to expand; thus, the primary lever is to optimize how existing capacity is deployed. By quantifying shelter-level accessibility and unmet demand, our approach identifies high-need micro-areas within the camps and supports the relocation of facilities to maximize population coverage and reduce inequalities under realistic resource constraints. In addition, a distinguishing feature of this study is its gender-responsive analysis. Leveraging the 2022 gender-designated data, we compute

accessibility scores separately for female and male FDMNs, thereby capturing spatial disparities in service provision. This approach addresses the disproportionate barriers and health risks faced by women and girls, particular in settings where female-designated facilities are deprioritized under constrained budgets [22]. Where data permit, the framework is extensible to other at-risk groups, such as persons with disabilities, and can be applied to additional service networks, including health posts, learning centers, and distribution points, across diverse refugee camp settings.

2 Results

2.1 Segmentation performance evaluation

We benchmark our semi-supervised framework against the following baseline models. The comparison includes conventional methods previously employed in refugee camp detection [23, 16], such as fully supervised architectures—U-Net [24], Fully Convolutional Network (FCN) [25], and UNetFormer [26]—as well as a semi-supervised framework (UniMatch-V2 [27]). In addition, we evaluate test-time adaptation techniques, including TENT [28] and SHOT [29], which represent recent approaches designed to address challenges associated with limited labeled data and domain shift. Table 1 presents the segmentation results evaluated using intersection over union (IoU), precision, recall, and F1-score, which are commonly used metrics for assessing segmentation performance. Across all metrics, the proposed method consistently outperforms all other approaches.

Fully supervised models demonstrate strong performance when ample labeled data are available; however, they overlook important structural cues and reach subpar segmentation accuracy in visually complex scenes. While UniMatch-V2 seeks to overcome this limitation by incorporating unlabeled data, its reliance on pseudo-labels generated by a teacher model renders it vulnerable to domain shifts. This leads to spatial misrepresentations that propagate systematic errors during training, ultimately constraining the long-term effectiveness of semi-supervised learning. Test-time adaptation methods such as TENT and SHOT aim to address domain shifts by adjusting model parameters during inference—minimizing entropy or maximizing mutual information. Yet, their dependence on self-generated predictions without explicit structural guidance similarly results in error accumulation. In contrast, our method enhances structural fidelity by refining teacher predictions using SAM (Segment Anything Model; see Methods Section), which selectively filters unreliable outputs while preserving semantically and structurally coherent regions (see Supplementary Text A.1). This yields cleaner supervision and consistently improves segmentation performance, as reflected in higher IoU and F1-scores.

Table 1: Segmentation performance on the refugee camp shelter class, evaluated using IoU, Precision, Recall, and F1-score across all baseline methods. Best scores are highlighted in bold with underline.

Method	IoU (%)	Precision (%)	Recall (%)	F1-score (%)
U-Net	60.1	63.8	78.4	70.3
FCN	61.5	65.2	<u>79.1</u>	71.5
UNetFormer	63.8	68.5	78.8	73.3
UniMatch-V2	65.0	71.0	73.2	72.1
SHOT	65.8	72.3	73.5	72.9
TENT	66.5	71.5	75.4	73.4
Proposed (Ours)	<u>69.2</u>	<u>75.8</u>	77.0	<u>76.4</u>

To further assess the effectiveness of our work, we conduct a qualitative comparison with baselines on unlabeled imagery collected in 2025, covering three distinct shelter density scenarios: high-density camp (#1), mid-density camp (#2), and low-density camp (#3). Representative examples from each category are provided in Figure 1.

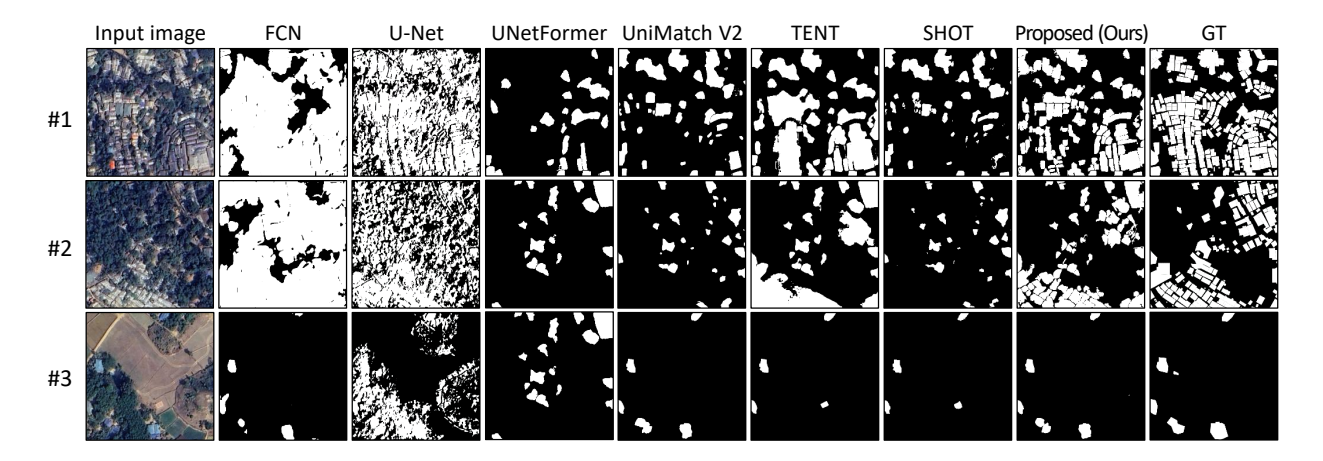


Figure 1: Representative segmentation results for high-density (#1), mid-density (#2), and low-density (#3) camps, comparing our method with baselines. Compared to other baselines, our model produces results that more closely resemble the ground-truth (GT) label, effectively handling the complex visual challenges of dense tree canopy noise, congested arrangements, and irregular shelter shapes.

In high- and mid-density cases (#1 and #2), most baselines produce inaccurate masks due to visual noise from dense tree canopies, severe spatial congestion, and irregular shelter geometries. Specifically, FCN, U-Net, and UNetFormer tend to yield fragmented or noisy predictions, frequently misclassifying vegetation as shelters. UniMatch-V2, TENT, and SHOT reduce false positives, mainly in areas of dense vegetation, but lack precise distinction of individual shelters, tending to merge adjacent shelters or omit smaller ones. In contrast, our method accurately separates closely spaced shelters while preserving sharp boundaries, even in heavily cluttered scenes. In the low-density case (#3), the baselines except U-Net perform reliably. Nevertheless, our method still achieves the fewest false negatives and the sharpest boundaries. These results indicate that our method offers clear advantages in high- and mid-density settings, delivering segmentation maps that maintain semantic accuracy and fine structural detail under complex camp conditions.

2.2 Changes in detected refugee shelters

Figure 2 presents the spatial and demographic changes of refugee shelters in Cox's Bazar over time. Panels A through D show the distribution of shelters detected in 33 camps in the district, highlighting those present in 2017 (marked in black), newly added in 2018 (blue), and further expansions by 2025 (red). The outward dispersion of colors reflects a consistent trend of camp expansion toward peripheral areas, observed across all sites. The blue bar chart in Panel E illustrates the changes in the total area of refugee shelters within the study region. The chart combines area estimates derived from UAV-based detection (2017 and 2018), satellite imagery analysis (2022 and 2025), manually digitized shelter outlines provided by UNOSAT and REACH (2020 and 2021) [17]. Overlaid in black, the line chart depicts shelter area normalized by the total population of FDMNs [5], expressed in square meters per individual, providing a comparative metric of living space per person over time.

The bar chart indicates a pronounced expansion in the camp area over time, with the most substantial increase (almost doubling) occurring between 2017 and 2018. This surge corresponds to the onset of the 2017 Rohingya Crisis, which caused a rapid and large-scale displacement of individuals from Myanmar to Bangladesh. The sudden influx overwhelmed existing infrastructure in the Cox's Bazar District, where facilities were not adequately prepared to accommodate arriving individuals. Consequently, living space per person in 2017 was limited to just 3.74 square meters, indicating extremely limited private space for basic needs such as sleeping, sanitation, and personal hygiene.

After 2020, the extent of the shelter stabilized, followed by a modest decline observed in subsequent years. This trend may reflect coordinated efforts of international agencies to formalize camp layouts and enhance infrastructure for long-term habitation. Episodic fire events also contributed to localized reductions in shelters [30]. Despite this spatial stabilization, the refugee population has continued to grow rapidly, resulting in a steady decline in living space per person—from 8.52 m² in 2020 to 7.33 m² in 2025. This figure remains above the UNHCR emergency standard of 3.5 m² per person in tropical climates [2], but it falls below the higher standards of living conditions, such as those of OECD countries with a range of 8 m² and 10 m² per person. The divergence between population growth and the available living space, which does not grow proportionally with the population but has stabilized, led to increasing density, with potential implications for overcrowding and diminished access to essential services.

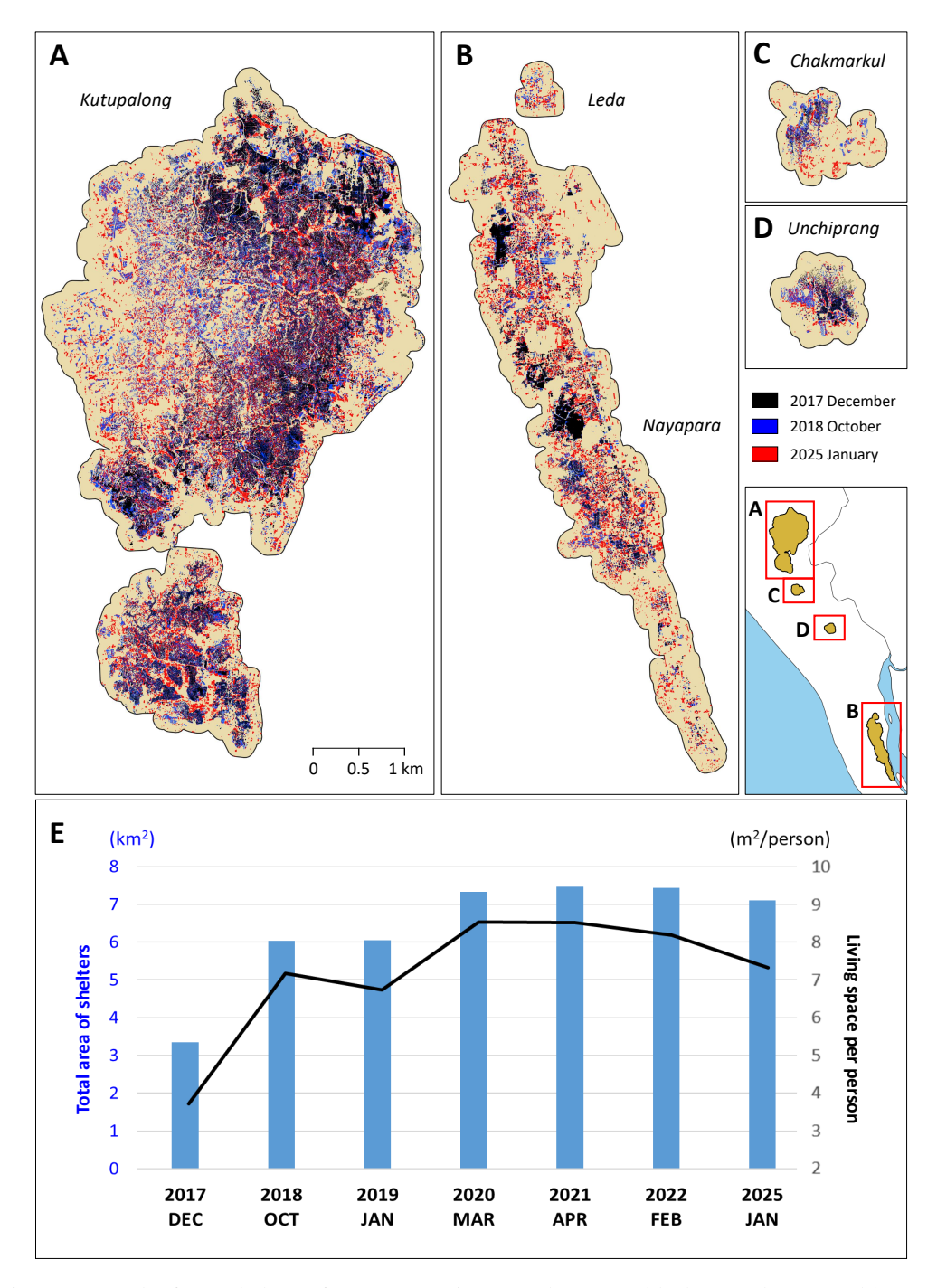


Figure 2: (**A-D**) Detected refugee shelters of Cox's Bazar in December 2017 (black), October 2018 (blue), and January 2025 (red). (**E**) Blue bars displays the total area of refugee shelters across seven time points, as estimated by our model (2017, 2018, 2022, and 2025) and ground-truth data (2020 and 2021). A black line indicates the living space per person (m² per person).

2.3 Change in accessibility to WASH facilities

Accessibility between demand and supply was calculated using the 2SFCA method based on network distances and aggregated to the 50-meter grid level (Figure 3). The supply was defined as the number of WASH facilities, while the demand was estimated from detected shelters weighed by camp population at a 50-meter grid (see Supplementary

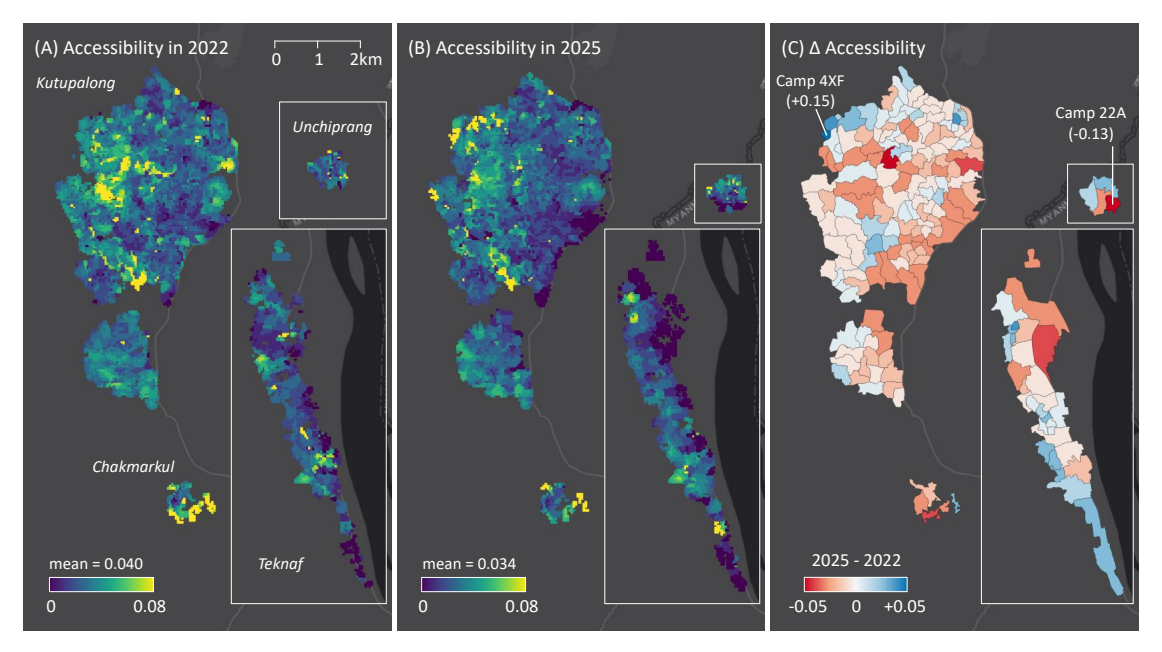


Figure 3: Accessibility to WASH facilities based on network distances in 2022 (**A**) and 2025 (**B**), and their change (**C**). Accessibility scores represent the mean accessibility of water pumps, latrines, and bathing cubicles. Changes are summarized at the camp block administrative level. Blue indicates areas where accessibility improved between 2022 and 2025, while red indicates areas where accessibility declined.

Text A.3 for details). Accessibility was calculated separately for each of the three types of WASH facilities and then averaged to a single accessibility value for 2022 (**A**) and 2025 (**B**). The difference between the two values was summarized at the administrative level of the camp block and used to assess changes in accessibility. In Figure 3 C, red indicates the accessibility was measured lower in 2025 compared to 2022, while blue represents higher accessibility. Accessibility based on Euclidean distances was also calculated (see Supplementary Figure 10. The overall trends are similar; however, the network distance–based analysis reveals more detailed variations at the local level.

The average accessibility score of WASH in all refugee camps decreased by approximately 0.006, from 0.040 in 2022 to 0.034 in 2025. This change corresponds to a scenario in which a population of 1,000 people had access to 40 facilities in 2022, but only 34 facilities in 2025. In contrast, each facility served an average of 25 people in 2022, compared to 29.4 people in 2025. This indicates that within three years, each facility now serves around four more people than before, suggesting a significant deterioration in WASH service conditions in Cox's Bazar. This number is higher than the global average of 24 refugees per toilet in 2024, based on data from 104 settlements in 17 countries [31]. Similar trends are observed in all types of facilities (see Supplementary Figure 11). A water pump now serves 67.1 people, compared to 47.8 people in 2022; a latrine serves 17.2 people, 2.2 more people than three years ago; and a bathing cubicle serves 32.9 people, compared to 30.7 people in 2022.

The changes in accessibility varied spatially between the camp blocks (Figure 3 C). The greatest declines were observed in the eastern part of Kutupalong and the southern part of Unchiprang (e.g., Camp 22A), with an average decrease of 0.12 (around 13 more people using one facility). In contrast, the greatest accessibility improvements occurred in Block F of Camp 4X in the northern part of Kutupalong, with an average increase of 0.15 (nearly 14 fewer people using one facility). These variations can be attributed to a combination of rapid population growth and reduced facility availability. Interestingly, the areas with the greatest declines did not experience the highest population growth. Instead, the main driver of the reduced accessibility in these camps was the minimal increase in the number of facilities (see Supplementary Figure 12).

To validate our accessibility scores, we compared the 2025 accessibility results with camp-level survey data on WASH facilities [32]. The Rohingya Refugee Response (RRR) conducted a WASH Sector Gap Analysis in September 2024, reporting the number of people per functional latrine in 33 camps in Cox's Bazar. These data serve as ground-truth information for local access to sanitation facilities. We then compared these figures with our averaged 2025 accessibility scores to latrines, yielding a Spearman's correlation coefficient of 0.709 (see Supplementary Figure 13).

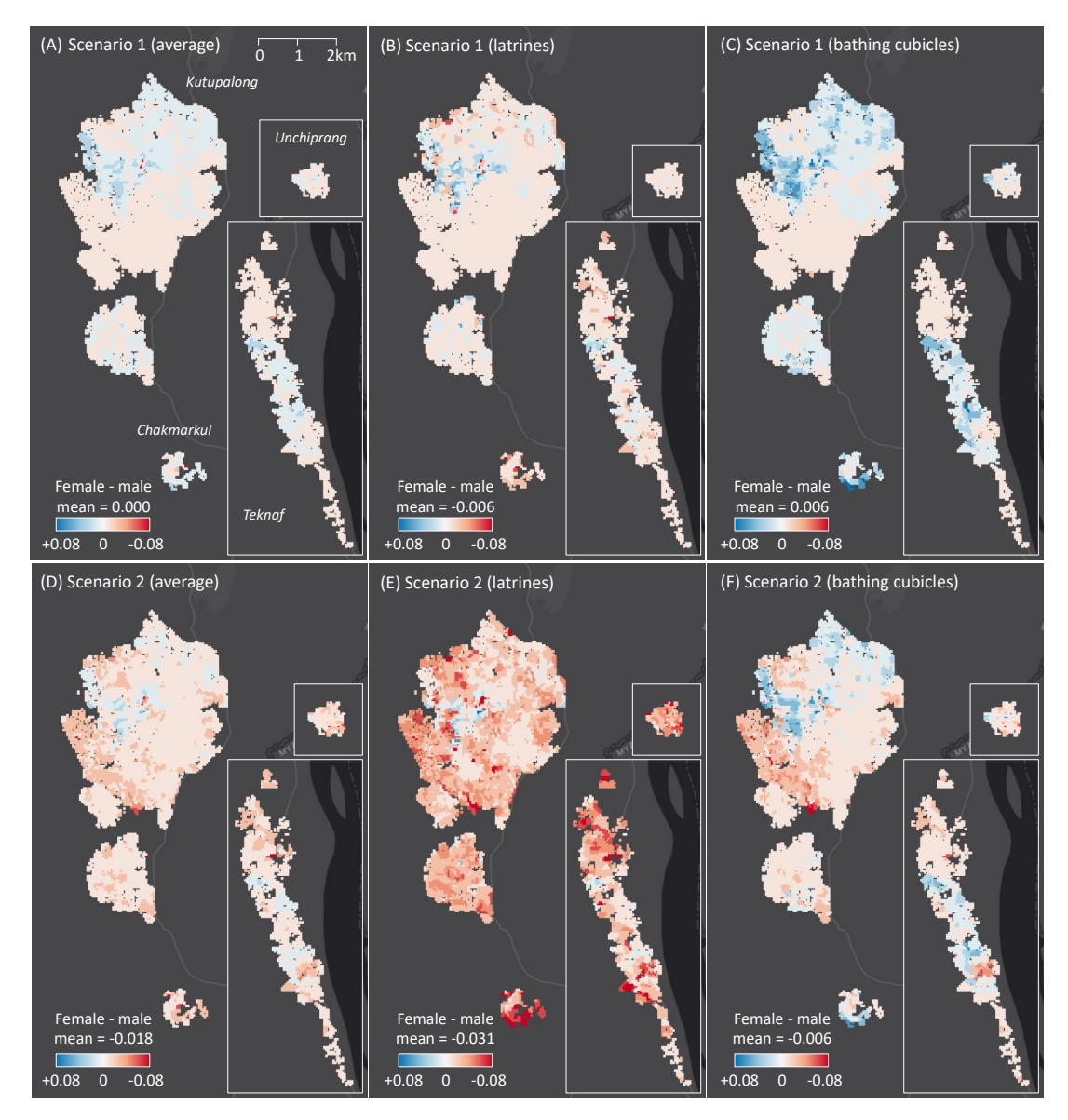


Figure 4: Gender-disaggregated accessibility analysis: average in three facilities (**A**, **D**), latrines (**B**, **E**), and bathing cubicles (**C**, **F**). Blue indicates relatively higher accessibility for women and girls, while red indicates relatively higher accessibility for men and boys. Scenario 1 (**A**–**C**) assumes that females are not reluctant to use all-gender facilities. Scenario 2 (**D**–**F**) assumes that 25% of females are reluctant to use all-gender facilities, based on thresholds derived from survey data [32].

2.4 Gender disparities in WASH accessibility

Our gender-disaggregated analysis reveals that women potentially face greater difficulties in assessing WASH facilities compared to men under certain conditions. As illustrated in Figure 4, accessibility scores differ by gender, reflecting variations in the number of female- and male-designated facilities as well as differences in population distribution of two groups. Blue indicates a relatively higher accessibility for women and girls, while red indicates a relatively higher accessibility for men and boys. To reflect real-world conditions, we developed two scenarios representing varying degrees of female FDMNs' use of all-gender WASH facilities. Scenario 1 (Figure 4 A–C) assumes that all females are willing to use all-gender facilities, sharing latrines and bathing cubicles with males. In contrast, 2022 survey data from a local organization [32] indicate that 25% of females in Cox's Bazar feel unsafe using communal latrines at night due to potential gender-based violence. Accordingly, Scenario 2 (D–F) applies a 25% reduction to the effective supply capacities of all-gender facilities when used by females, to account for this reluctance.

In Scenario 1, the overall accessibility scores show no significant gender difference, with values of 0.0661 for females and 0.0659 for males. For latrines, female accessibility scores are slightly lower than those for males (0.115 versus 0.121), despite the construction of more women-designated latrines (6,284; see Table 2 in Materials) compared to men-designated latrines (5,396). This disparity likely reflects the larger female population, which constitutes 51.5% of the refugee camp population [5]. For bathing cubicles, women have a higher accessibility score (0.062) compared to men (0.056), a difference that can be attributed to the greater number of female-designated cubicles (4,505) compared to male-designated cubicles (395). However, the vast majority of bathing cubicles (21,075) are not segregated and women may face constraints using such facilities. Scenario 1, thus, may not accurately represent real-world accessibility conditions.

In Scenario 2, where females encounter barriers when using all-gender facilities, the average accessibility scores indicate significantly higher male accessibility (0.066) compared to female accessibility (0.048). This scenario assumes that each gender-separated WASH facility is shared by an average of 20.8 females and 15.2 males. On average, each latrine serves 11.1 females or 8.3 males, while each bathing cubicle serves 20.3 females and 18.0 males. These figures underscore significant gender disparities in WASH service conditions in Cox's Bazar. Spatially, the central and northern areas of Kutupalong—where Rohingya central administrative facilities are concentrated—provide relatively better WASH accessibility for women (highlighted in blue in Figure 4 F). However, accessibility for women declines progressively toward more peripheral areas (highlighted in red in E).

3 Discussion

Humanitarian planning for refugee crises requires accurate and up-to-date geospatial data on the location and extent of individual camp structures; however, such information is largely unavailable in refugee contexts [33]. Satellite imagery and UAVs provide consistent, wide-area coverage and enable timely mapping in regions where ground-based surveys are infeasible [34]. Nevertheless, detecting structures within refugee camps under emergency conditions poses greater challenges compared to regularly planned camps. Emergent camps exhibit extremely high shelter densities and low geometric alignment, with structures built in close proximity and minimal spacing between them. Dense vegetation obstructs rooftop visibility, further complicating the segmentation of individual buildings. The Rohingya refugee camps in Cox's Bazar illustrate these difficulties: rapid, unplanned expansion has produced dense, uneven, and heterogeneous settlement morphologies that defy conventional detection techniques [15].

This noisy setting underscores the value of our proposed approach for a more robust refugee camp mapping in humanitarian crises. By integrating SAM into the segmentation framework, we achieve a more reliable detection of camp structures in complex environments in comparison to other approaches. Unlike conventional models, which are hindered by visual noise from dense vegetation, spatial congestion, and irregular shelter geometries, our approach preserves both semantic accuracy and fine-grained structural detail. These advantages are particularly pronounced in high- and medium-density settings, where existing methods frequently fail. Beyond performance improvements, our findings suggest that structural guidance provides a generalizable strategy to improve segmentation under challenging conditions.

We applied our segmentation results to quantify public health conditions in refugee camps. Utilizing the 2SFCA metric, we mapped camp structures and assessed temporal and gender-based disparities in WASH accessibility between 2022 and 2025. Our findings reveal a critical decline over time in both total and per capita availability of WASH facilities, driven by population growth and stagnant infrastructure expansion. The decline in accessibility underscores the importance of incorporating sub-district level demographic data into infrastructure planning. Relying on static indicators such as facility count alone can obscure the growing inequalities in service provision. Accessibility should not only be measured in terms of physical presence, but also in relation to demand. As our findings suggest, service equity can be improved by optimizing the placement of WASH facilities based on population distribution and patterns. In settings of fixed or shrinking budgets, a demand-responsive allocation—guided by geospatial analysis—can identify critical under-served areas and ensure that limited infrastructure serves the greatest number of people, with a particular emphasis on vulnerable groups.

In addition, our gender-disaggregated analysis of WASH accessibility provides empirical evidence that contributes to the broader discourse on gender inequities in humanitarian contexts [35]. Many female refugees shoulder disproportionate caregiving responsibilities, while cultural barriers frequently restrict their opportunities to work, own property, or pursue education. Safety concerns are widespread, with increased risks of gender-based violence (GBV) both within and outside of camp environments. The results show that women and girls generally have lower WASH accessibility than men and boys, particularly with respect to latrine access. Promoting gender equity requires not only the installation of additional facilities, but also the provision of separate facilities for men and women to ensure safety, privacy, and equitable access [36]. Only 22.2% of the latrines and 18.9% of the bathing cubicles are gender-separated in the Rohingya

camp. Even in gender-separated facilities, these designations are often disregarded, largely due to long waiting times for toilet use [7]. This sharing potentially increases the risk of GBV, which predominantly affects women [37]. However, our scenario-based approximations require further refinement through future studies that incorporate data on behavior, perceived and measured risks for women, and other potentially overlooked factors in Rohingya and other camp settings.

Given recent financial reductions in international aid, such as the defunding of USAID programs [38], it is likely that the conditions and maintenance of the WASH facilities in the Rohingya refugee camps will deteriorate further in the coming years. This trajectory reflects a broader fragility in refugee settlements worldwide, where dependence on external funding continues to expose essential services to systemic risk. The trends observed in Cox's Bazar, marked by shrinking infrastructure, overcrowding, and declining accessibility, have high possibilities to recur in camps throughout Kenya, Uganda, or South Sudan [39]. As our method is transferable to other refugee contexts [23], these findings underscore the need for scalable monitoring frameworks capable of tracking service degradation and supporting locally adaptable interventions in protracted displacement settings.

4 Materials

The Rohingya refugee camps are located in the Ukhiya and Teknaf *Upazilas* (sub-districts) of Cox's Bazar District in southeastern Bangladesh (Figure 5). These sub-districts border Myanmar's Rakhine State, the origin of mass displacement following violent persecution in 2017. As a result, the region now hosts one of the largest concentrations of refugee settlements worldwide. A total of 33 registered camps are currently distributed in Ukhiya and Teknaf (indicated as green areas on the map), the majority are clustered near the Kutupalong site in Ukhiya, one of the largest refugee camps globally [1]. One camp previously located in Shamlapur (Camp 23) was relocated to Bhasan Char, an island outside Cox's Bazar, in December 2021. To maintain consistency in spatial analysis, this relocated site is excluded from the present study.

In addition to registered camps, several unregistered Rohingya settlements remain pending formal validation. These unregistered FDMNs reside in areas characterized by informal, irregular layouts, and limited access to essential services. Although they host a significant portion of the refugee population, these settlements are excluded from the present analysis due to the lack of consistent and comprehensive data. Official facility data sets and those documenting latrines are only available for registered camps, where humanitarian interventions are implemented more systematically. Therefore, this study focuses on the 100-meter buffered extents of registered camps (outlined in red in Figure 5 A, B) to ensure consistency and reliability in spatial and infrastructural assessments.

Within the defined limits, four datasets were used to infer accessibility to WASH facilities in the Rohingya refugee camps (Figure 6). The refugee shelter outlines were identified using UAV and satellite imagery in seven temporal snapshots. Then these detected shelters were spatially linked to the facility location data to assess access to WASH services. As facility data were available only for the years 2022 and 2024, accessibility analysis is restricted to these two time points.

4.1 Refugee shelter outline data

We obtained geospatial building outline data on refugee shelters from the Humanitarian Data Exchange (HDX) [17], a service provided by the United Nations Office for the Coordination of Humanitarian Affairs (OCHA). The outline data are derived from UAV imagery captured by the International Organization for Migration (IOM) and processed by REACH/UNOSAT. OCHA provides multi-temporal datasets of refugee shelters from February 2018 to April 2021. Some datasets, including those from February 2018, provide only partial coverage of Rohingya refugee camps, and no publicly accessible updates have been released since.

Three temporally distinct datasets of refugee shelters, compiled in February 2018, January 2019, and April 2021, were employed to support model training. These shelter labels served as ground-truth annotations for imagery acquired in December 2017, October 2018, and February 2022, respectively. The outline data includes a range of building features within the camps, including self-built bamboo, tarpaulin, and concrete shelters (Figure 5 E). In certain instances, misalignment was observed between labels and images, attributable to temporal offsets, which we separately handled using a correction algorithm in the data training process (see Section 5.1.1).

4.2 UAV imagery

The UAV imagery was acquired by the Needs and Population Monitoring initiative of the IOM Bangladesh [40], which aims to support international efforts to assess the evolving conditions of the Rohingya refugee population. We obtained

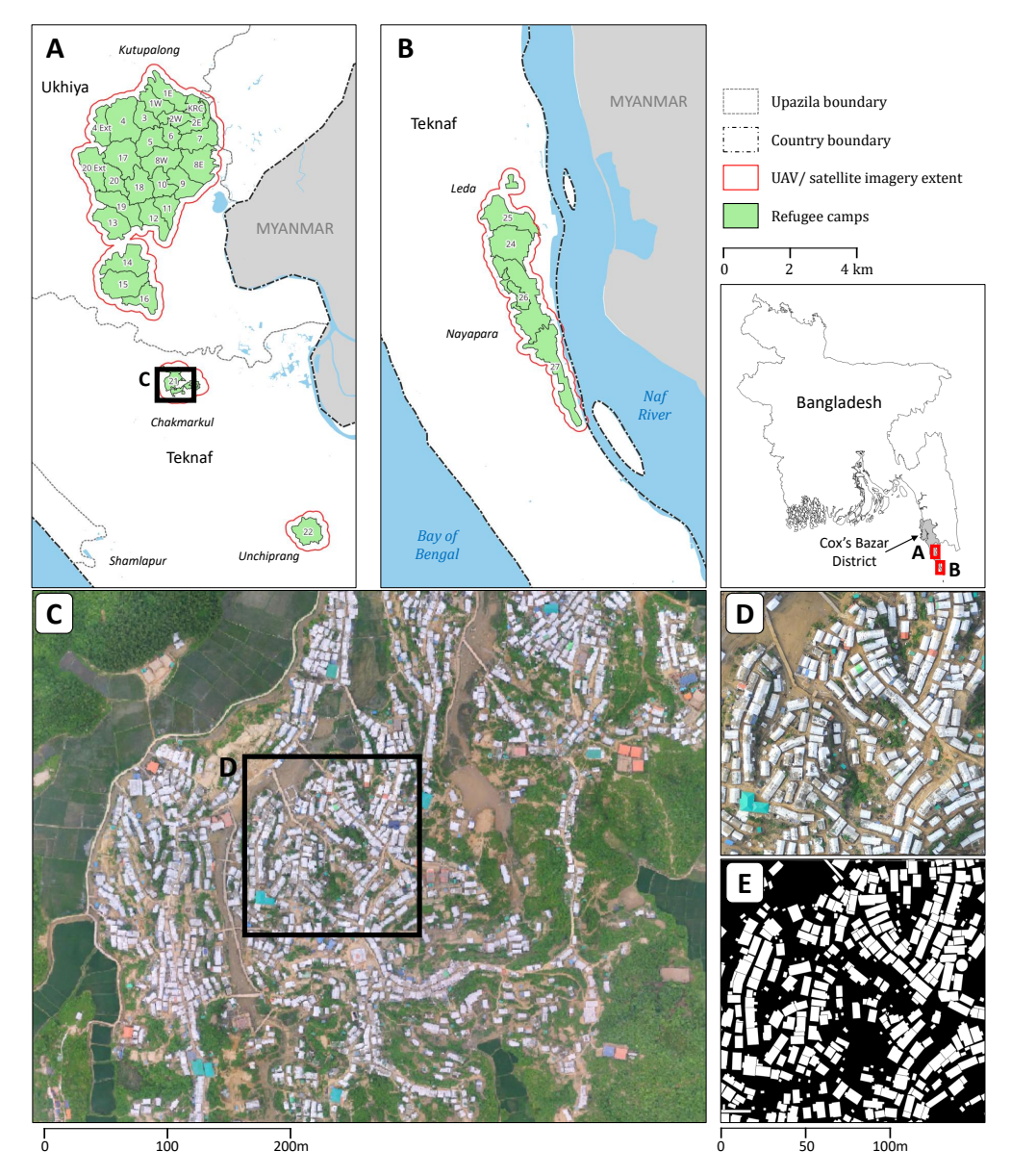


Figure 5: Outlines of the 33 Rohingya refugee camps (shown in green) and the extent of UAV/satellite imagery used for the segmentation framework (indicated by red borders). The camps are located in the Ukhiya (**A**) and Teknaf (**B**) *Upazilas* (sub-districts) within Cox's Bazar, southeastern Bangladesh. The names of the refugee camps are labeled above the outlines. Camp boundary data, compiled on May 19, 2024, were sourced from the Inter Sector Coordination Group (ISCG). UAV imagery from Camp 21 in Chakmarkul (**C**) provides an example of a Rohingya refugee shelter layouts. Zoomed-in views in (**D** and **E**) illustrate examples of input imagery and corresponding ground-truth labels of shelter outlines for the segmentation model.

two temporal UAV imagery data from the HDX website, captured in December 2017 and October 2018. These images were aligned with refugee shelter outline data from February 2018 and January 2019.

We adopted a standardized resolution for imagery data based on the zoom level resolution system, commonly used by online satellite imagery platforms such as Google Maps. In this system, each zoom level corresponds to a fixed ground sampling distance (resolution in meters per pixel). At zoom level 0, the entire Earth is represented as a single 256×256-pixel image. With each increase in zoom level, the spatial resolution doubles and the Earth is divided into four times as many images. For example, at zoom level 18, the Earth is partitioned into approximately 68 billion images, with a resolution finer than 60 centimeters per pixel, sufficient to distinguish individual building structures. This system

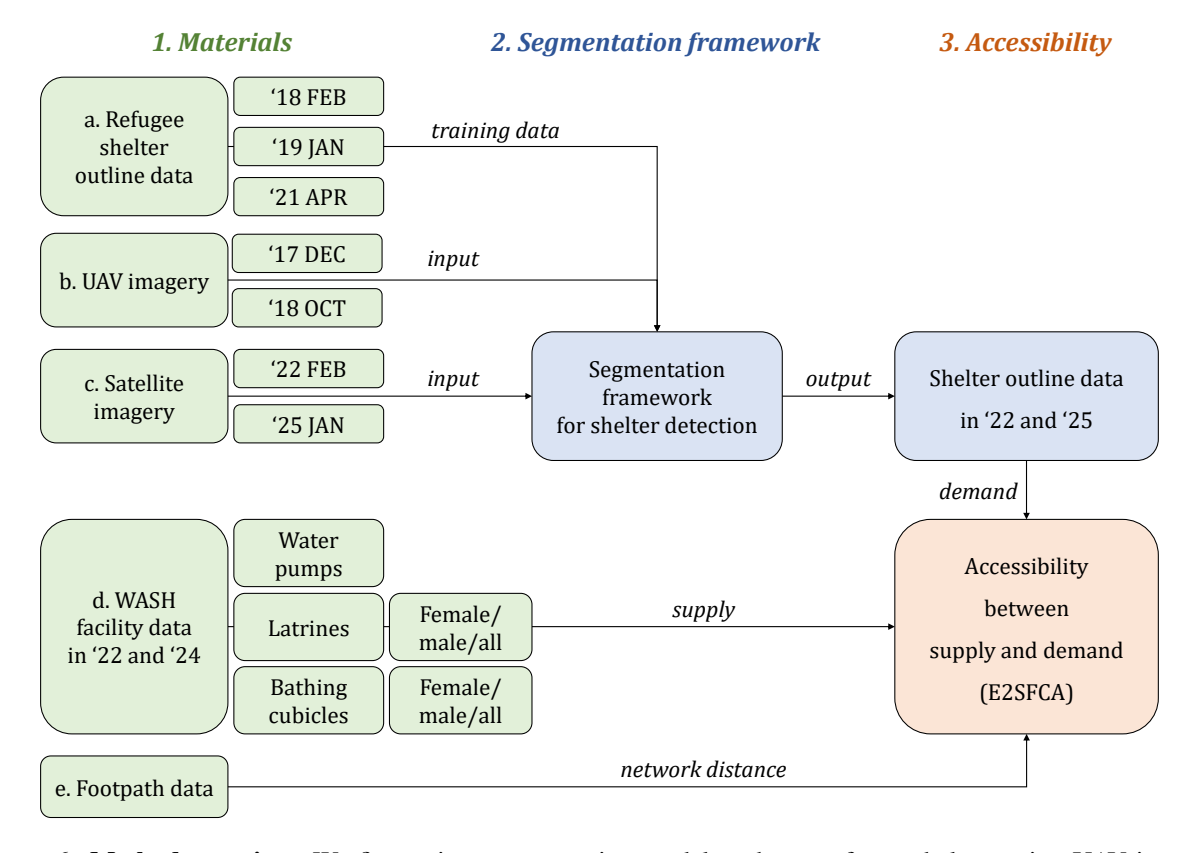


Figure 6: **Method overview.** We first train a segmentation model to detect refugee shelters using UAV imagery downsampled at zoom level 18 (60 centimeters per pixel), with manually annotated shelter outlines serving as ground-truth labels. The model is then used to satellite imagery in 2022 and 2025 to predict shelter outlines. The second step is to measure accessibility from the detected shelters to three types of geolocated WASH facilities—water pumps, latrines, and bathing cubicles—for the years 2022 and 2024. The 2022 facility data are further categorized by gender (male, female, and all-gender), enabling comparative analysis of accessibility by gender. The walking network distance between shelters and facilities is calculated with footpath data.

enables a standardized extent and resolution framework for remote sensing imagery, facilitating the integration of diverse datasets such as UAV and satellite images.

The original spatial resolution of the UAV imagery is 10 centimeters per pixel. The images were then divided into non-overlapping images of 256×256 pixels. The true color images have three values per pixel, representing the red, green, and blue (RGB) spectral bands. To ensure compatibility with satellite imagery, which typically has lower resolution, we downloaded a downsampled version of the UAV imagery at zoom level 18. Example data is shown in Figure 5 (**D**), where refugee shelters are easily visible at this resolution. In total, 7,406 UAV image tiles were generated over the two years.

4.3 Satellite imagery

The UAV data for several years are missing, resulting in temporal gaps in high-resolution coverage. Consequently, high-resolution satellite images captured in the past three years have been used as an alternative in such cases. Satellite images at zoom level 18 were downloaded for two time points: February 2022 and January 2025. We retrieved the Maxar (GE01) image captured in 2022 from the ESRI World Imagery Wayback using the ESRI ArcGIS REST API (https://livingatlas.arcgis.com/wayback/). Additionally, an Airbus image from 2025 was obtained using Google Earth Engine. The 2022 dataset was aligned with the shelter outline data from April 2021 to jointly train the framework with UAV imagery. In total, 7,406 satellite image tiles were generated over two years.

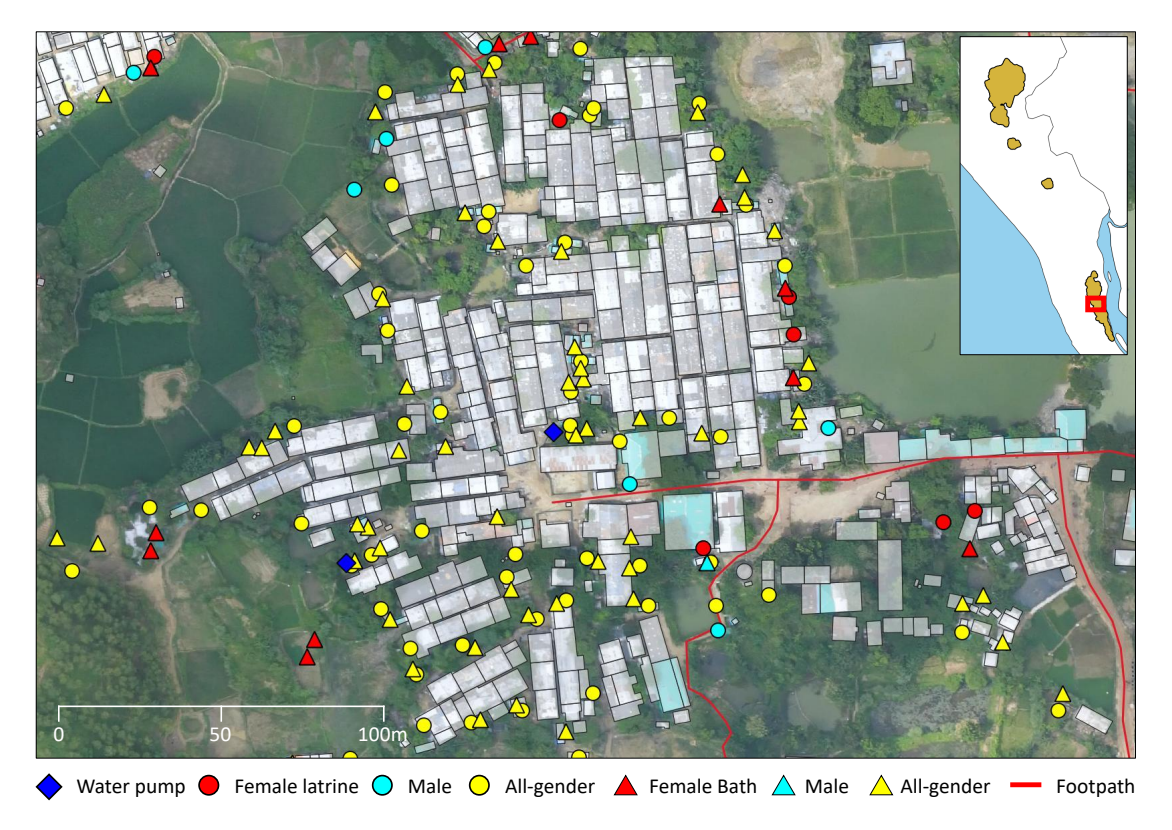


Figure 7: Neighborhood map of water pumps (quadrangles), latrines (circles), and bathing cubicles (triangles) in 2022 for Camp 26, Teknaf. Latrines and bathing cubicles are classified by gender designation.

4.4 Facility location data

Geospatial data on WASH infrastructure were obtained from the Rohingya Refugee Response (RRR), which provides facility-level coordinates and metadata (e.g., type and size) for all camps as of May 2022 and August 2024 [12]. This dataset was selected for its comprehensive coverage that spans all camp areas. Facilities are categorized into three types—water pumps, latrines, and bathing cubicles—capturing a range of WASH services (Figure 7). Although some data points also extend outside the boundaries of the camp, we restricted our analysis to facilities within the camp area to control data quality. The May 2022 data were paired with satellite imagery from February 2022, and the August 2024 data with imagery from January 2025. Shapefiles are publicly accessible via the official repository.

Table 2 presents summary statistics for three types of WASH facilities at two time points. "Location" refers to a geographic point where one or more facilities are co-located. A facility is defined as an individual physical unit of WASH infrastructure, such as a single tube well. The number of facilities in each location represents its size of the WASH infrastructure. On average, each location has 1 water pump, 1.42–1.53 latrines, and 1.25–1.32 bathing cubicles.

The absolute number of all three types of facilities decreased between 2022 and 2024. A key factor behind this decline is the reduction in international aid and funding [41]. Thousands of facilities have been decommissioned due to underfunding, leading to aging infrastructure and limited maintenance. In addition, the number of facilities per 100 people decreased between 2022 and 2024, indicating a reduced per capita availability of WASH infrastructure over time. This decrease is attributed to an increase in the refugee population, which grew from 899,867 in May 2022 to 958,614 in August 2024. This decrease has occurred despite efforts by the international community to expand the WASH facilities.

Gender-disaggregated data are available only for latrines and bathing cubicles in 2022. In both cases, the number of female-designated facilities exceeds that of male-designated facilities. This reflects a greater focus of Rohingya camp organizations on empowering women and girls in the WASH sector [42]. The need for women-only facilities has been emphasized as a means of reducing the incidence of sexual violence against women and girls in WASH facilities. According to a survey conducted in 2022 [32], only 75% of women reported feeling safe using communal latrines at night. While there are many dedicated men's latrines (5,396), the number of men's bathing cubicles is relatively small

(395), suggesting that men are more likely than women to use the all-gender bathing cubicles (21,075). Accessibility scores by gender were calculated by including facilities for each gender category, as well as all-gender facilities.

	2022 May			2024 August		
	Water pump	Latrine	Bath cubicle	Water pump	Latrine	Bath cubicle
Total locations	17,639	34,343	19,623	15,620	37,057	20,686
Total facilities	17,661	52,635	25,974	15,620	52,495	25,805
Facilities per location	1.01	1.53	1.32	1.00	1.42	1.25
Facilities for female	_	6,284	4,504	_	_	_
Facilities for male	_	5,396	395	_	_	_
Facilities for all genders	_	40,955	21,075	_	_	_
Facilities per 100 people	1.96	5.84	2.89	1.63	5.48	2.69

Table 2: Summary statistics for three types of WASH facilities in 2022 and 2024.

Note: "Location" indicates a geographic point with one or more WASH facilities, each defined as a single unit of infrastructure (e.g., tube well, latrine stall, bath cubicle). Facility count per location reflects infrastructure scale.

4.5 Footpath data

The walking distance between detected shelters and facilities is necessary to calculate the accessibility score. We compute network distances along a pedestrian network derived from the Rohingya Refugee Response footpath dataset (September 2025 release; Figure 7) [43]. Shelter centroids and facility locations were snapped to the nearest network vertex or edge, while calculating their offsets. The pairwise network distances were then computed using the shortest single-source path. The total distance with offsets is used for the accessibility metric.

5 Methods

5.1 Segmentation Framework for Refugee Shelter Detection

Problem Setting. We consider a small set of labeled data $\mathcal{L} = \{(x_i, y_i)\}_{i=1}^{N_1}$, where each image $x_i \in \mathbb{R}^{H \times W \times 3}$ is paired with a corresponding binary mask $y_i \in \{0,1\}^{H \times W}$, along with a larger set of unlabeled data $\mathcal{U} = \{x_j\}_{j=1}^{N_u}$. In the binary mask, each pixel is labeled as Background (class 0) or Refugee Shelter (class 1). Our objective is to train a model f that estimates a binary mask g from an image g.

Overview. Our method follows a student-teacher paradigm, which is particularly effective for semi-supervised learning in segmentation tasks with limited labeled data. In this framework, the teacher model provides initial guidance derived from unlabeled data to the student model, enabling the student to learn more reliably by incorporating this guidance throughout the training process. Each model takes an image as input x and returns a probability map p = f(x), which is converted to a binary mask \hat{y} via thresholding. Due to spatial misalignments (e.g., image distortion and geometric errors) within the labeled data, an alignment pre-processing step is applied before training, as detailed in Section 5.1.1. The teacher model f_{θ_t} is first pre-trained on the labeled data using a standard cross-entropy loss:

$$\mathcal{L}_{\text{Sup}} = \frac{1}{N_l} \sum_{i=1}^{N_l} \text{CE}(f_{\theta_t}(x_i), y_i), \tag{1}$$

After training, the teacher model generates coarse predictions \hat{y}^t for the unlabeled images. These predictions are refined using a pre-trained Segment Anything Model (SAM) [44] g, whose zero-shot capability boosts instance-segmentation performance across unfamilar scenes in which the teacher model can fail to recognize objects. This produces more accurate pseudo-labels \tilde{y} that serve as a supervisor for predictions \hat{y}^s of the student model f_{θ_s} , as detailed in Section 5.1.2. To further mitigate the distribution shift between training and test data, we adopt the test-time adaptation. Specifically, the student model is optimized on the unlabeled data using a combination of a segmentation loss and an entropy-based regularization for test-time adaptation:

$$\mathcal{L}_{\text{Unsup}} = \frac{1}{N_u} \sum_{j=1}^{N_u} \text{CE}(f_{\theta_s}(x_j), \tilde{y}_j) + \frac{1}{N_u} \sum_{j=1}^{N_u} \mathcal{H}(f_{\theta_s}(x_j)), \tag{2}$$

where $\mathcal{H}(p) = -\sum_k p_k \log p_k$, with indexing k classes, denotes the Shannon entropy [45]. To gradually improve pseudo-label quality, the teacher model is updated via an exponential moving average (EMA) of the student model's parameters:

$$\theta_t \leftarrow \alpha \cdot \theta_t + (1 - \alpha) \cdot \theta_s \tag{3}$$

Here, α is a decay rate typically set close to 1, and θ_t and θ_s are the teacher and student parameters, respectively.

Motivation. Our goal is to detect refugee shelters from UAV and satellite imagery, despite two major challenges: (i) limited availability of pixel-level annotations, and (ii) significant domain shifts between training and test distributions. Figure 8 provides an overview of our proposed semi-supervised framework designed to address these challenges.

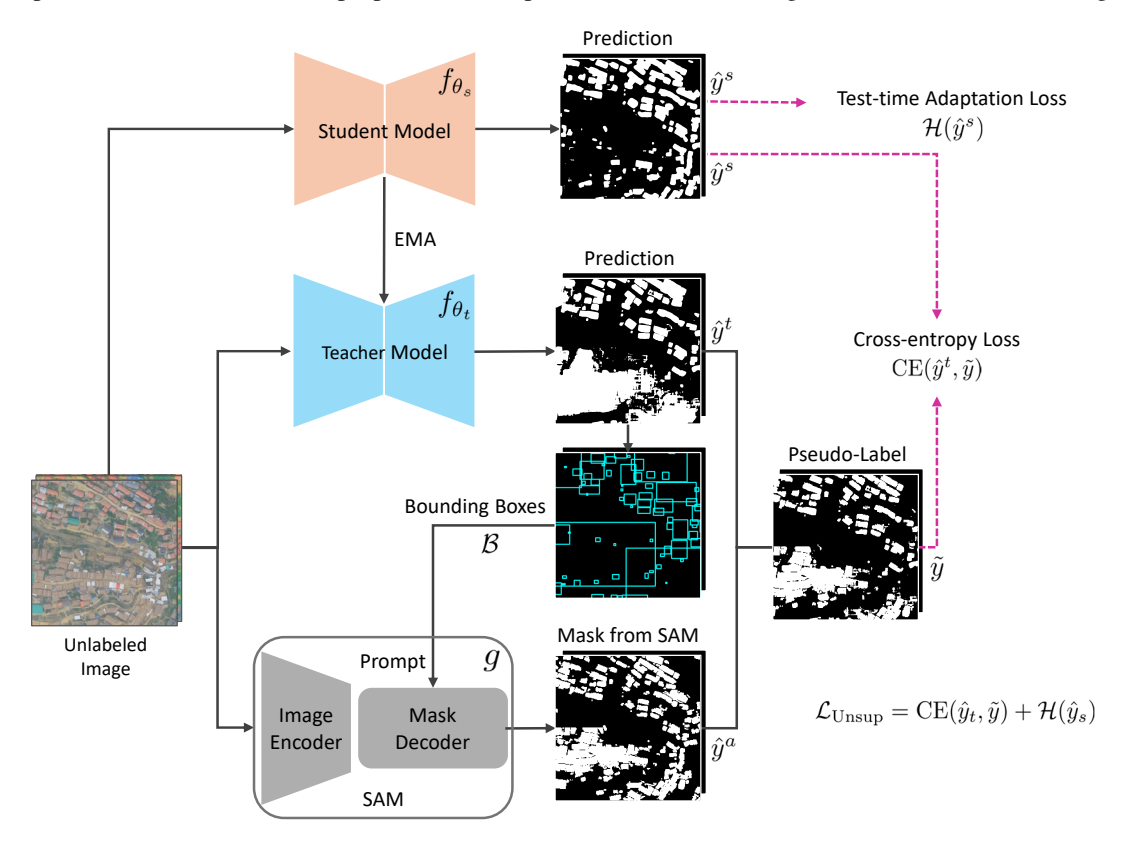


Figure 8: Overview of the proposed semi-supervised segmentation framework for refugee shelter detection. The teacher model f_{θ_t} is first trained on labeled data. It then generates coarse predictions \hat{y}_t for unlabeled images, which are refined using a guided Segment Anything Model (SAM) g with bounding-box prompts \mathcal{B} to produce accurate pseudo-labels \tilde{y} . The student model f_{θ_s} is optimized to minimize the loss function $\mathcal{L}_{\text{Unsup}}$, composed of a cross-entropy term (CE) between its predictions \hat{y}_s and the refined pseudo-labels, with an entropy regularization term (\mathcal{H}) on \hat{y}_s for domain adaptation. The teacher is updated via an exponential moving average of the student's weights, progressively improving pseudo-label quality.

5.1.1 Alignment via SAM-based Structural Matching

To correct spatial misalignments in the labeled data, we adopt an efficient alignment strategy that uses masks from SAM as structural references. For each labeled image x_i with its mask y_i , we obtain a reference mask \hat{y}_i^a from SAM g, which highlights regions likely to correspond to shelter buildings. A discrete search is performed on integer translations $(\Delta u, \Delta v) \in [-R_t, R_t]^2$ and rotations $\theta \in [-R_r, R_r]$, where Δu and Δv denote horizontal and vertical pixel shifts, and θ denotes rotation in degrees, to maximize the F1-score between the transformed mask $T_{(\Delta u, \Delta v, \theta)}(y_i)$ and the reference mask \hat{y}_i^a :

$$F1(\Delta u, \Delta v, \theta) = \frac{2 \cdot |\hat{y}_i^a \cap T_{(\Delta u, \Delta v, \theta)}(y_i)|}{|\hat{y}_i^a| + |T_{(\Delta u, \Delta v, \theta)}(y_i)|} \tag{4}$$

The optimal transformation is obtained as:

$$(\Delta u^*, \Delta v^*, \theta^*) = \arg \max_{(\Delta u, \Delta v, \theta)} F1(\Delta u, \Delta v, \theta), \tag{5}$$

This transformation is applied identically to both the image x_i and its mask y_i . Specifically, empty regions created by the transformation are padded with zeros in both the images and the masks. This approach ensures robust alignment across diverse images using SAM's structural signals, even without precise labels or additional training.

5.1.2 Pseudo-Label Refinement with SAM

To enhance the reliability of pseudo-labels, we refine teacher model's outputs using SAM on the unlabeled data. In dense and irregular shelter arrangement, these initial predictions frequently fail to clearly separate adjacent instances or capture small and occluded ones, resulting in merged or missed detections. SAM can segment closely packed objects with high spatial precision and also handle visual ambiguities caused by atypical shelter buildings. However, its capability depends on suitable prompts, particularly for localizing individual shelters. To effectively guide SAM, we extract bounding boxes \mathcal{B} from the prediction \hat{y}_j^t of the teacher model f_{θ_t} and use them as a spatial prompt for SAM g, enabling it to generate a structure-based mask \hat{y}_i^a :

$$\hat{y}_j^a = g(x_j; \mathcal{B}). \tag{6}$$

The final pseudo-label \tilde{y}_i is computed by intersecting the teacher's prediction and the guided SAM mask:

$$\tilde{y}_j = \hat{y}_j^t \cap \hat{y}_j^a. \tag{7}$$

This intersection helps reduce false positives from SAM, especially in the early stages of training, when coarse predictions may lead to oversized bounding boxes. By retaining only the regions agreed upon by both models, it gives more reliable supervision signals to train the student model f_{θ_s} .

5.2 Measuring accessibility to WASH facilities

In recent decades, accessibility studies have developed various metrics to measure spatial relationships between populations and service providers [21]. These include simple container-based measures, which calculate provider-to-population ratios within administrative boundaries, and distance-based measures, which consider travel times or distances to the nearest facilities. From the 1990s onward, gravity models gained prominence by integrating both, provider capacity and distance decay functions, offering a more accurate representation of spatial interaction [19]. Building on this tradition, the two-step floating catchment area (2SFCA) became widely adopted in this domain for its balance of conceptual rigor and computational simplicity [20]. Its main strength lies in its two analytical steps, which systematically account for both supply and demand catchments. By considering both sides, the method effectively captures local competition between facilities and populations. Numerous extensions of 2SFCA have been proposed to introduce various distance decay functions, the sizes of the catchment areas, and the preference of customers [18], making accessibility measurement a continuously evolving research area.

Adopting the 2SFCA approach, we measure accessibility on a 50-meter grid using network distances, rather than at the level of individual detected shelters, to capture broader spatial trends within Cox's Bazar. The study computes accessibility three times for each type of WASH facility and then average them to produce overall accessibility scores. We define population and facility sets $\mathcal{I} = \{i\}_{i=1}^{N_p}$ and $\mathcal{J} = \{j\}_{j=1}^{N_f}$, representing demand and supply locations, respectively. Each population point $i \in \mathcal{I}$ has an associated population size P_i , and each facility $j \in \mathcal{J}$ has a service capacity S_j (i.e., the number of WASH facilities). Population for each grid cell is estimated based on the total area of shelters within the grid, weighted by population data from 33 camps, including total and sex-disaggregated (female/male) populations [5] (see Supplementary Text A.3 for details). For every pair (i,j), let d_{ij} denote the travel distance or time between the population location i and the facility j.

We also consider a Gaussian distance-decay function:

$$K_{ij} = \begin{cases} \exp\left(-\frac{d_{ij}^2}{\sigma^2}\right), & \text{if } d_{ij} \le d_0, \\ 0, & \text{otherwise.} \end{cases}$$
 (8)

where σ controls the rate of distance decay. This decay function accounts for the fact that the influence of a facility decreases with increasing distance. By assigning smaller weights to farther locations, K_{ij} ensures that facilities closer to a population point contribute more to its accessibility, reflecting realistic spatial interactions within each catchment. A catchment threshold can be given differently for the type of facilities. However, we adopt one-mile threshold (1,609 m) as an acceptable walking distance to WASH facilities [46]. Consistent with findings in the literature, this function assigns a steep decline in weight values at 0.25 mile (402 m) [19].

In the first step of 2SFCA, the provider-to-population ratio for each facility j is defined as

$$R_j = \frac{S_j}{\sum_{i: d_{ij} \le d_0} P_i K_{ij}},\tag{9}$$

 R_j represents the service capacity available per person within the catchment area of facility j. It quantifies how much supply (i.e., service capacity) is available relative to the total nearby FDMN population that can reach that facility, summing over all population locations i with $d_{ij} \leq d_0$, each weighted by the distance with previously defined decay function. Higher R_j indicates less competition for that facility's services, while lower R_j reflects higher demand pressure or limited service capacity.

Then, the *accessibility score* at each population location i is

$$A_i = \sum_{j: d_{ij} \le d_0} R_j K_{ij}. \tag{10}$$

 A_i quantifies the overall accessibility experienced by the population at the location i, aggregating the weighted influence of all facilities within its catchment. It sums up all facilities j with $d_{ij} \leq d_0$, each weighted by the facility's service-to-population ratio (R_j) and the distance decay between i and j. In other words, A_i quantifies how much effective service capacity can be reached from a given population point. Higher values of A_i indicate better availability and proximity of the service, while lower values of A_i reflect limited access or longer travel distances to essential facilities.

Declarations

The authors declare no competing interests. Code to replicate the findings of this study is available at https://github.com/DS4H-GIS/Refugee_WASH_Accessibility.

References

- [1] iDMC. Global Report on Internal Displacement. Internal Displacement Monitoring Centre (iDMC), Geneva, Switzerland, 2025.
- [2] UNHCR. *Global Trends: Forced Displacement in 2024*. United Nations High Commissioner for Refugees (UNHCR), Copenhagen, Denmark, 2025.
- [3] Rohingya Refugee Response. 2024 joint response plan rohingya humanitarian crisis, 2025.
- [4] Malang Faye. A forced migration from myanmar to bangladesh and beyond: humanitarian response to rohingya refugee crisis. *Journal of international humanitarian action*, 6:1–7, 2021.
- [5] Operational Data Portal-Bangladesh. Operational data portal-bangladesh. https://data.unhcr.org/en/country/bgd, 2025. Accessed: 20 June 2025.
- [6] S. Butt, M. S. R. Chowdhury, S. Sadique, A. A. Faisal, A. Mahama, A. Gorski, B. Pop-Stefanija, D. Beversluis, J. M. Lochokon, K. Velivela, K. Uadiale, M. Rahman, T. G. Worku, T. J. G. Billiew, and P. Keating. Assessment of water, sanitation and hygiene services within nineteen rohingya camps in cox's bazar, bangladesh in 2022. *BMC Health Services Research*, 25(1):1–12, 2025.
- [7] Khusnur Jahan Shapna, Kamrul Hasan, Kazi Humayun Kabir, Jianfeng Li, and Md Lokman Hossain. Water, sanitation and hygiene challenges of forcibly displaced myanmar nationals in rohingya camps in bangladesh. *Journal of Water and Health*, 21(10):1385–1403, 2023.
- [8] Iulia Toma, Mita Chowdhury, Mushfika Laiju, Nina Gora, and Nicola Padamada. *Rohingya refugee response gender analysis: recognizing and responding to gender inequalities.* Oxfam, Oxford, UK, 2018.
- [9] Mehereen Akhter, Sayed Mohammad Nazim Uddin, Nazifa Rafa, Sanjida Marium Hridi, Chad Staddon, and Wayne Powell. Drinking water security challenges in rohingya refugee camps of cox's bazar, bangladesh. *Sustainability*, 12(18):7325, 2020.
- [10] Salma Akter, Tapan Kumar Dhar, Abid Ibna A Rahman, and Md Kamal Uddin. Investigating the resilience of refugee camps to covid-19: A case of rohingya settlements in bangladesh. *Journal of migration and health*, 4:100052, 2021.

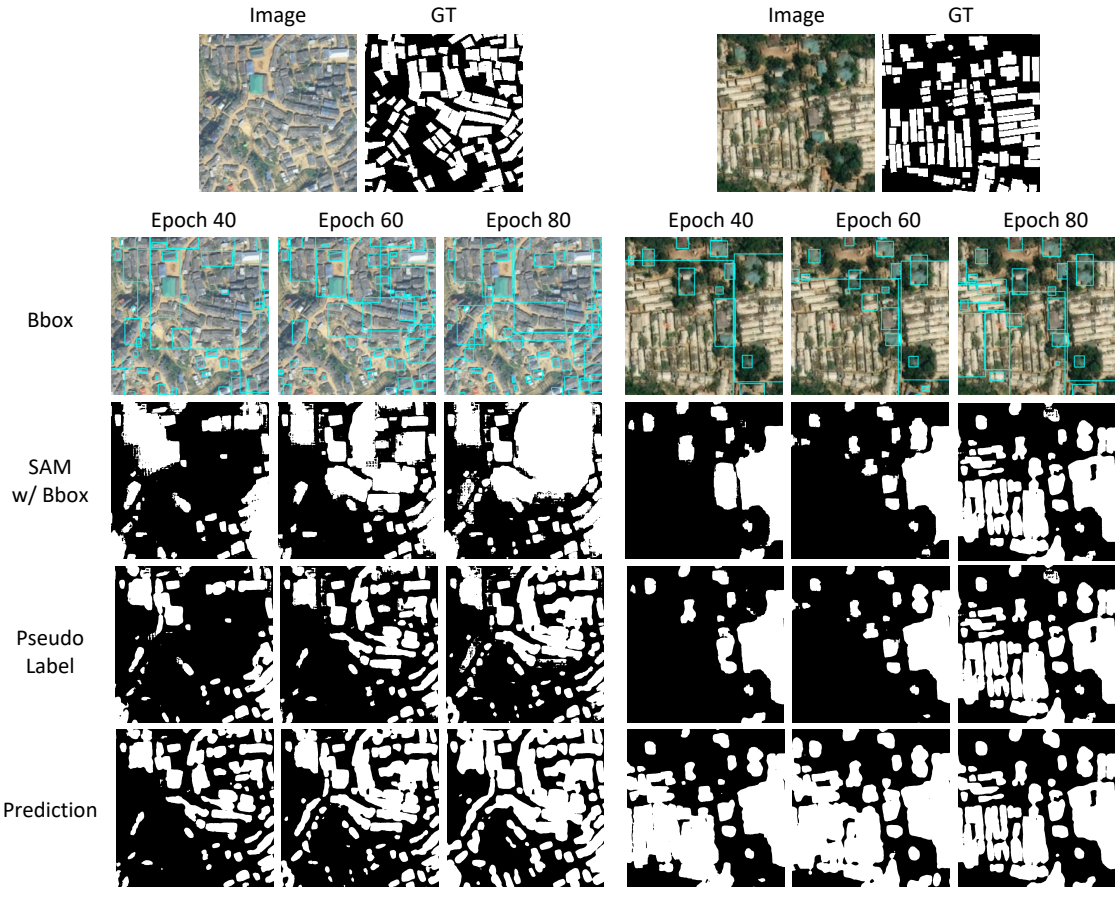
- [11] ASG Faruque, Baharul Alam, Baitun Nahar, Irin Parvin, Ashok Kumar Barman, Soroar Hossain Khan, M Nasif Hossain, Yulia Widiati, ASM Mainul Hasan, Minjoon Kim, et al. Water, sanitation, and hygiene (wash) practices and outreach services in settlements for rohingya population in cox's bazar, bangladesh, 2018–2021. *International Journal of Environmental Research and Public Health*, 19(15):9635, 2022.
- [12] Rohingya Refugee Response. Water, sanitation and hygiene (wash) cox's bazar. https://rohingyaresponse.org/sectors/coxs-bazar/wash/, 2025. Accessed: 8 July 2025.
- [13] J. A. Quinn, M. M. Nuhan, C. Navarro, D. Coluccia, L. Bromley, and M. Luengo-Oroz. Humanitarian applications of machine learning with remote-sensing data: review and case study in refugee settlement mapping. *Philosophical Transactions A*, 376:20170363, 2018.
- [14] Yunya Gao. Leveraging segment anything model in identifying buildings within refugee camps (sam4refugee) from satellite imagery for humanitarian operations. *arXiv preprint arXiv:2407.11381*, 2024.
- [15] M. Weigand, S. Worbis, M. Sapena, and H. Taubenböck. A structural catalogue of the settlement morphology in refugee and idp camps. *International Journal of Geographical Information Science*, 37(6):1338–1364, 2023.
- [16] O. Ghorbanzadeh, A. Crivellari, D. Tiede, P. Ghamisi, and S. Lang. Mapping dwellings in idp/refugee settlements using deep learning. *Remote Sensing*, 14(24):6382, 2022.
- [17] Reach Initiative. Cox's bazar district refugee camp structure/shelter/infrastructure footprints. https://data.humdata.org/dataset/bangladesh-refugee-camp-structure-footprint-march-2020, 2021. Accessed: 20 June 2025.
- [18] Wei Luo and Yi Qi. An enhanced two-step floating catchment area (e2sfca) method for measuring spatial accessibility to primary care physicians. *Health & place*, 15(4):1100–1107, 2009.
- [19] James Bryant Jr and Paul L Delamater. Examination of spatial accessibility at micro-and macro-levels using the enhanced two-step floating catchment area (e2sfca) method. *Annals of GIS*, 25(3):219–229, 2019.
- [20] X. Chen and P. Jia. A comparative analysis of accessibility measures by the two-step floating catchment area (2sfca) method. *International Journal of Geographical Information Science*, 33(9):1739–1758, 2019.
- [21] Jinwoo Park and Daniel W Goldberg. A review of recent spatial accessibility studies that benefitted from advanced geospatial information: multimodal transportation and spatiotemporal disaggregation. *ISPRS International Journal of Geo-Information*, 10(8):532, 2021.
- [22] Strategic Executive Group. JRP for Rohingya Humanitarian Crisis. UN OCHA, Cox's Bazar, Bangladesh, 2018.
- [23] Katrin Wernicke. Deep Learning for Refugee Camps-Mapping Settlement Extents with Sentinel-2 Imagery and Semantic Segmentation. PhD thesis, University of Würzburg, 2023.
- [24] O. Ronneberger, P. Fischer, and T. Brox. U-net: Convolutional networks for biomedical image segmentation. In *Proceedings of the International Conference on Medical Image Computing and Computer-Assisted Intervention (MICCAI)*, pages 234–241, Cham, 2015. Springer.
- [25] Jonathan Long, Evan Shelhamer, and Trevor Darrell. Fully convolutional networks for semantic segmentation. In *Proceedings of the IEEE Conference on Computer Vision and Pattern Recognition (CVPR)*, pages 3431–3440, Boston, 2015. IEEE.
- [26] L. Wang, R. Li, C. Zhang, S. Fang, C. Duan, X. Meng, and P. Atkinson. Unetformer: A unet-like transformer for efficient semantic segmentation of remote sensing urban scene imagery. *ISPRS Journal of Photogrammetry and Remote Sensing*, 190:196–214, 2022.
- [27] Lihe Yang, Zhen Zhao, and Hengshuang Zhao. Unimatch v2: Pushing the limit of semi-supervised semantic segmentation. *IEEE Transactions on Pattern Analysis and Machine Intelligence*, 2025. arXiv preprint arXiv:2410.10777.
- [28] Dequan Wang, Evan Shelhamer, Shaoteng Liu, Bruno Olshausen, and Trevor Darrell. Tent: Fully test-time adaptation by entropy minimization. In *International Conference on Learning Representations (ICLR)*, 2021.
- [29] Jian Liang, Dapeng Hu, and Jiashi Feng. Do we really need to access the source data? source hypothesis transfer for unsupervised domain adaptation. In *International Conference on Machine Learning (ICML)*, pages 6028–6039, Virtual Event, 2020. PMLR.
- [30] Mohammad Mehedy Hassan, Ikramul Hasan, Jane Southworth, and Tatiana Loboda. Mapping fire-impacted refugee camps using the integration of field data and remote sensing approaches. *International Journal of Applied Earth Observation and Geoinformation*, 115:103120, 2022.
- [31] UNHCR. WASH Annual Report 2024. United Nations High Commissioner for Refugees (UNHCR), Copenhagen, Denmark, 2024.

- [32] Rohingya Refugee Response. Overview and monitoring of wash per camp (round 5, updated october 31, 2024). https://rohingyaresponse.org/wp-content/uploads/2024/11/Overview-and-Monitoring-of-WASH-Per-Camp_Round_5_October-31_2024.pdf, 2025. Accessed: 8 July 2025.
- [33] Patrick Aravena Pelizari, Kristin Spröhnle, Christian Geiß, Elisabeth Schoepfer, Simon Plank, and Hannes Taubenböck. Multi-sensor feature fusion for very high spatial resolution built-up area extraction in temporary settlements. *Remote sensing of environment*, 209:793–807, 2018.
- [34] M. Burke, A. Driscoll, D. B. Lobell, and S. Ermon. Using satellite imagery to understand and promote sustainable development. *Science*, 371(6535):eabe8628, 2021.
- [35] Heaven Crawley. Gender, 'refugee women' and the politics of protection. In *The palgrave handbook of gender and migration*, pages 359–372. Springer, Cham, 2021.
- [36] Fatine Ezbakhe, Ricard Giné-Garriga, and Agustí Pérez-Foguet. Leaving no one behind: Evaluating access to water, sanitation and hygiene for vulnerable and marginalized groups. *Science of the total environment*, 683:537–546, 2019.
- [37] GBVSS. GBVIMS Factsheet, Q1 2025 Cox's Bazar January-March 2025. Rohingya Refugee Response, Cox's Bazar, Bangladesh, 2025.
- [38] Daniella Medeiros Cavalcanti, Lucas de Oliveira Ferreira de Sales, Andrea Ferreira da Silva, Elisa Landin Basterra, Daiana Pena, Caterina Monti, Gonzalo Barreix, Natanael J Silva, Paula Vaz, Francisco Saute, et al. Evaluating the impact of two decades of usaid interventions and projecting the effects of defunding on mortality up to 2030: a retrospective impact evaluation and forecasting analysis. *The Lancet*, 2025.
- [39] Alhelí Calderón-Villarreal, Ryan Schweitzer, and Georgia Kayser. Social and geographic inequalities in water, sanitation and hygiene access in 21 refugee camps and settlements in bangladesh, kenya, uganda, south sudan, and zimbabwe. *International journal for equity in health*, 21(1):27, 2022.
- [40] IOM Bangladesh. Needs and population monitoring (npm) cox's refugees settlements uav imagery. https://data.humdata.org/dataset/ bangladesh-refugee-camp-structure-footprint-march-2020, 2025. Accessed: June 2025.
- [41] UNICEF, WASH Briefing Note 2025. WASH Sector CXB, Cox's Bazar, Bangladesh, 2025.
- [42] ISCG. Gender Tip Sheet and Gender Policy (Bangla) WASH. Inter Sector Coordination Group (ISCG), Cox's Bazar, Bangladesh, 2021.
- [43] Rohingya Refugee Response. Resources & data. https://rohingyaresponse.org/resources-data/, 2025. Accessed: 8 July 2025.
- [44] Alexander Kirillov, Eric Mintun, Nikhila Ravi, Hanzi Mao, Chloe Rolland, Laura Gustafson, Tete Xiao, Spencer Whitehead, Alexander C Berg, Wan-Yen Lo, et al. Segment anything. In *Proceedings of the IEEE/CVF international conference on computer vision*, pages 4015–4026, 2023.
- [45] John C. Baez, Tobias Fritz, and Tom Leinster. A characterization of entropy in terms of information loss. *Entropy*, 13(11):1945–1957, 2011.
- [46] Yong Yang and Ana V Diez-Roux. Walking distance by trip purpose and population subgroups. *American journal of preventive medicine*, 43(1):11–19, 2012.
- [47] Daniel Delling, Andrew V. Goldberg, Andreas Nowatzyk, and Renato F. Werneck. Phast: Hardware-accelerated shortest path trees. In 2011 IEEE International Parallel & Distributed Processing Symposium, pages 921–931, 2011.

Appendix A Supplementary Text

A.1 Effectiveness of SAM-guided pseudo-label Refinement

We evaluate the impact of SAM-based pseudo-label refinement by tracking intermediate and final segmentation outputs across training epochs. Figure 9 presents examples from a high-density camp in UAV imagery (left) and satellite imagery (right).



* The model was trained using only labeled data up to epoch 40.

Figure 9: Progressive results of the proposed method with SAM-guided pseudo-label refinement across training epochs for a high-density camp in UAV (left) and satellite (right) data.

In both modalities, refinement progressively sharpens object boundaries, improves the separation of closely spaced shelters, and recovers small or partially occluded structures that are initially missed by the teacher model. Despite the lower spatial resolution of satellite imagery compared to UAV imagery — which increases visual noise — the method still preserves fine structural details and reduces false positives. These results demonstrate that the refinement using SAM effectively addresses the various visual challenges inherent to camp detection. By providing strong structural priors, it enables accurate shelter delineation and reliable recovery of ambiguous structures, thereby mitigating common limitations of conventional pseudo-labeling.

A.2 Implementation details for segmentation framework

We configure UNetFormer [26] as the backbone for both teacher and student models. The labeled data consists 2,418 UAV and 1,721 satellite images, while the unlabeled dataset consists 4,988 UAV and 5,685 satellite images. For pre-training, we follow a 9:1 split on the labeled data. During training, images are randomly cropped to 768×768 to improve diversity and robustness, while evaluation is performed on original size 1024×1024 images. All pre-processing and data augmentation follow the official UNetFormer implementation. The teacher model is pre-trained for 40 epochs

on the labeled data using AdamW with a learning rate of $1\mathrm{e}{-4}$ and weight decay of 0.01. The student is then trained for an additional 40 epochs (80 in total) on unlabeled data with a reduced learning rate of $1\mathrm{e}{-5}$, maintaining the same weight decay. During training, the teacher is updated via an exponential moving average (EMA) of the student's parameters ($\alpha = 0.999$). All experiments are conducted with a batch size of 32.

Evaluation Metrics. Segmentation performance is assessed using Intersection over Union (IoU), Precision, Recall, and F1-score. All reported results are averaged over three random seeds to guarantee reliable evaluation.

Hardware. The experiment is performed on a single NVIDIA RTX 3090 GPU.

A.3 Implementation details for measuring accessibility

Grid-level population. To estimate the population at a 50-meter grid resolution, we allocate camp-level population data to grid cells based on our shelter detection results. First, we compute the total area of detected shelters within the administrative boundaries of the 33 camps. For each camp, the 2022 and 2025 population figures are divided by the total shelter area to derive the number of people per square meter of building area. This calculation is performed separately for the total, female, and male populations. Next, we estimate the population of each grid cell by multiplying the corresponding number of people per square meter by the area of detected shelters within that grid cell. When a grid cell overlapped multiple camp boundaries, population estimates are weighted according to the proportion of shelter area intersecting each camp, and the weighted values are summed. This interpolation approach is adopted because assessing accessibility by population provides a more intuitive representation of facility distribution relative to population than assessing accessibility by shelter areas.

Network distances. Footpath data are converted into an undirected network graph, with each edge weighted by its physical length (in meters) to enable computation of minimum travel distances along the pedestrian network. Grid-cell centroids (*demand nodes*) and WASH facility locations (*supply nodes*) are snapped to the nearest network vertex or edge to ensure topological connectivity. The Euclidean distance from each original point location to its snapping position on the network—referred to here as the *offset distance*—is added to the computed shortest-path length to obtain the total network distance. If the Euclidean distance between a demand node and a supply node is shorter than the sum of their respective offset distances, the Euclidean distance is used instead of the network-based distance. Shortest-path distances between each demand–supply pair are calculated along the network using the *parallel hardware-accelerated shortest path trees* (PHAST) algorithm [47].

Hardware and Software. The computations are performed in R (v4.5.0) on an Ubuntu (24.04 LTS) machine equipped with 12 CPU cores and 64 GB of RAM. The packages include terra, sf, sfnetworks, cppRouting, and RcppParallel. The projected coordinate system (EPSG:3857) is used to maintain metric consistency.

Appendix B Supplementary Figures

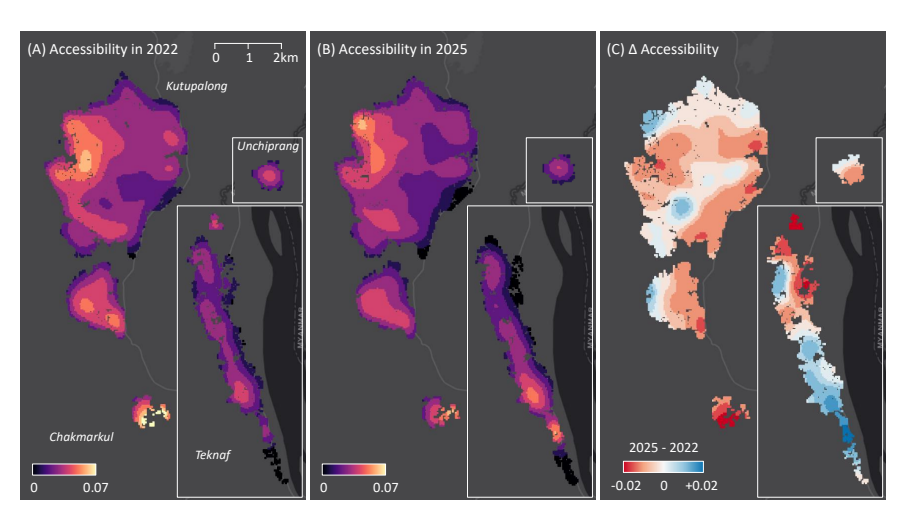


Figure 10: Accessibility to WASH facilities based on Euclidean distances in 2022 (A) and 2025 (B), and their change (C). Accessibility scores represent the mean accessibility of water pumps, latrines, and bathing cubicles.

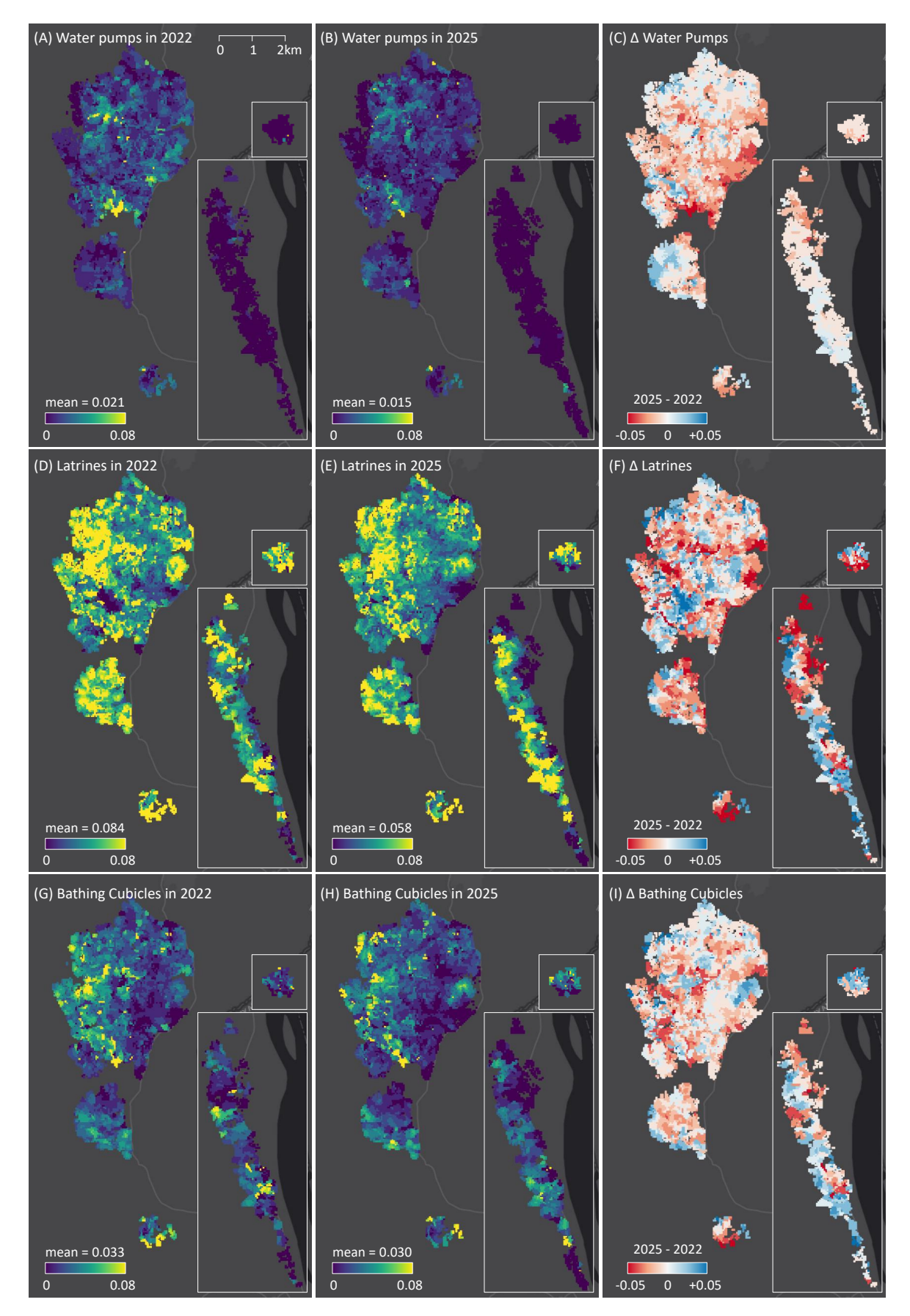


Figure 11: Accessibility based on network distances to water pumps (A-C), latrines (D-F), and bathing cubicles (G-I) in 2022, 2025, and the change between them.

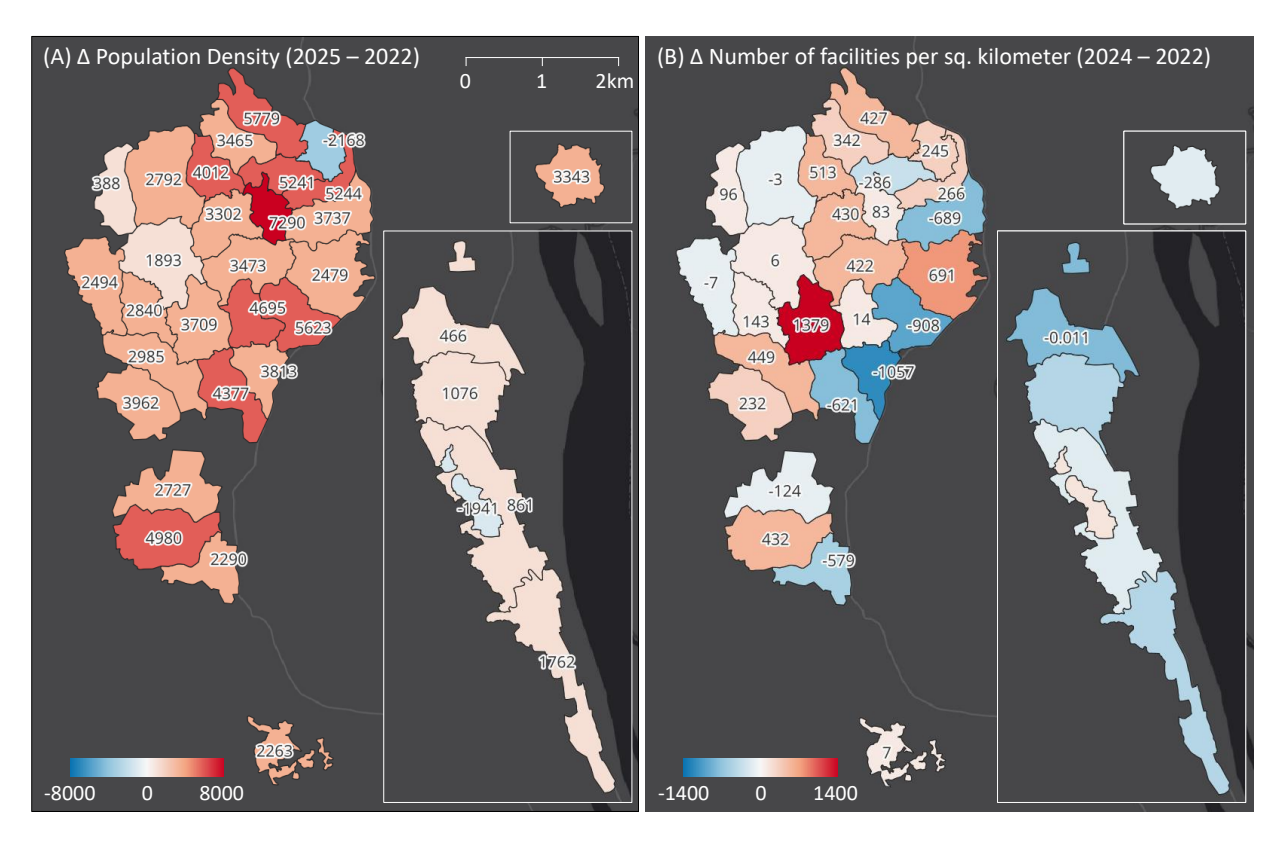


Figure 12: Changes in population density (A) and facility density (B) at the camp unit level. Population density is compared between 2022 and 2025, while facility density is compared between 2022 and 2024, reflecting the respective data availability periods.

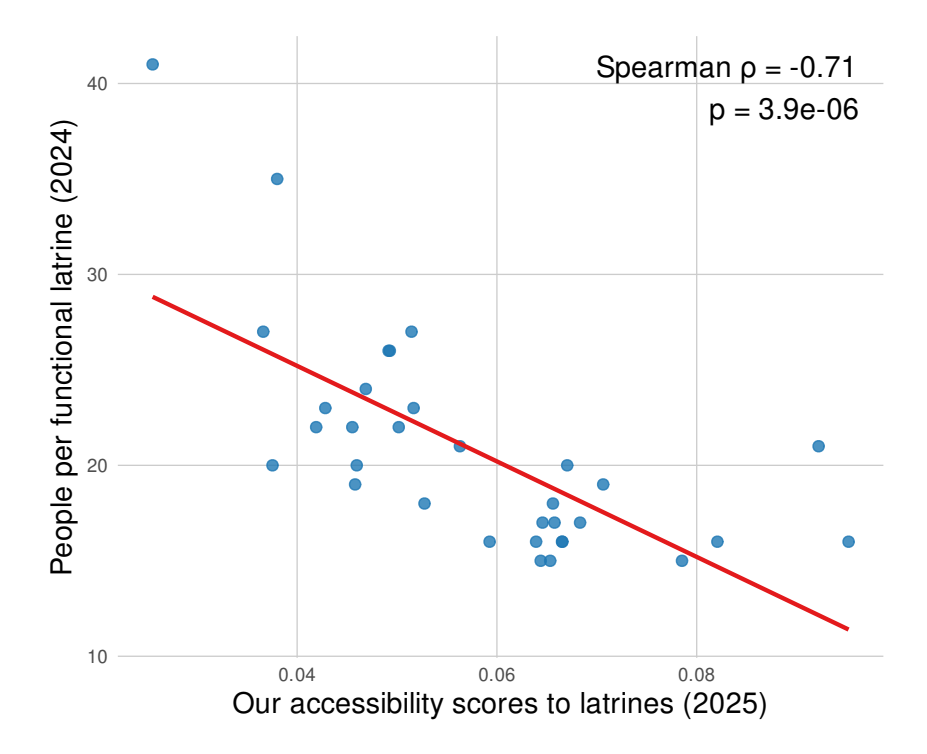


Figure 13: Comparison between our 2025 accessibility scores to latrines and survey-based data on people per functional latrines across 33 camps in Cox's Bazar [32]. The strong negative Spearman's correlation (ρ = -0.709) indicates a good agreement between the predictions of our model and the evaluations of local organizations in Cox's Bazar. Spearman's correlation was used because the variables did not meet the normality assumptions required for Pearson's correlation.